nature materials

SUPPLEMENTARY INFORMATION

https://doi.org/10.1038/s41563-017-0006-0

In the format provided by the authors and unedited.

Thermochromic halide perovskite solar cells

Jia Lin[1,2,3], Minliang Lai[1], Letian Dou[1,2,4], Christopher S. Kley[1], Hong Chen[1], Fei Peng[5], Junliang Sun[5], Dylan Lu[1,2], Steven A. Hawks[1,2,6], Chenlu Xie[1], Fan Cui[1], A. Paul Alivisatos[1,2,7,8], David T. Limmer[1,2,7] and Peidong Yang[1,2,7,8]*

[1]Department of Chemistry, University of California, Berkeley, California, USA. [2]Materials Sciences Division, Lawrence Berkeley National Laboratory, Berkeley, California, USA. [3]Department of Physics, Shanghai University of Electric Power, Shanghai, China. [4]Davidson School of Chemical Engineering, Purdue University, West Lafayette, Indiana, USA. [5]Berzelii Center EXSELENT on Porous Materials, Department of Materials and Environmental Chemistry, Stockholm University, Stockholm, Sweden. [6]Lawrence Livermore National Laboratory, Livermore, California, USA. [7]Kavli Energy NanoScience Institute, Berkeley, California, USA. [8]Department of Materials Science and Engineering, University of California, Berkeley, California, USA. Jia Lin, Minliang Lai and Letian Dou contributed equally to this work. *e-mail: p_yang@berkeley.edu

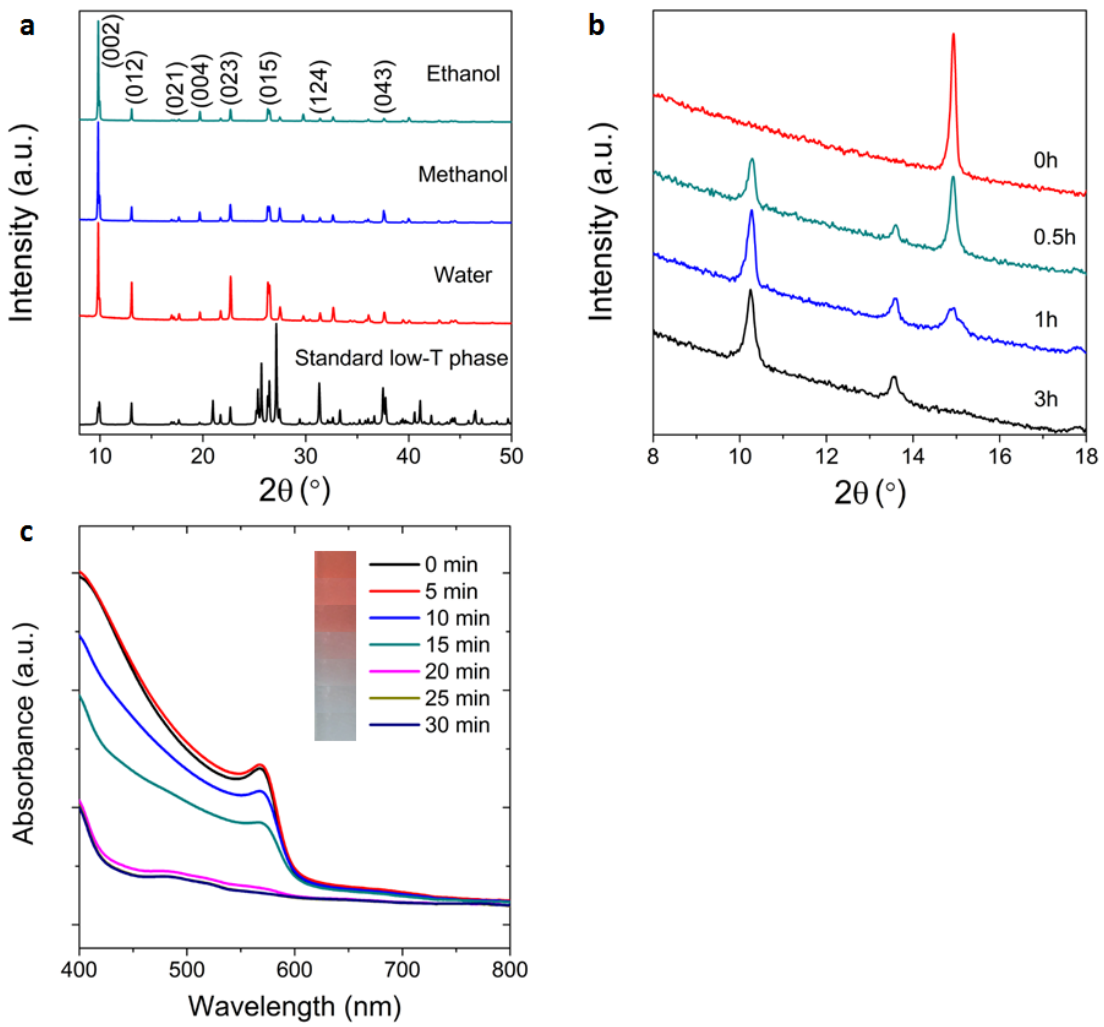

Supplementary Figure 1. The phase transitions and optical properties. a, XRD patterns of the low-T phase obtained by exposure to water, methanol, and ethanol vapors, and standard low-T phase of $CsPbI_3$. **b**, The evolution of the characteristic XRD peaks of $CsPbIBr_2$ film over time during the high-T to low-T phase transition at RH = 70% (high-T peak: 14.9 ° (100); low-T peaks: 10.3 ° (002) and 13.6 ° (012)). **c**, Absorbance spectra of $CsPbIBr_2$ as a function of exposure time at RH = 80% during the phase transition. The inset shows the color change of the film.

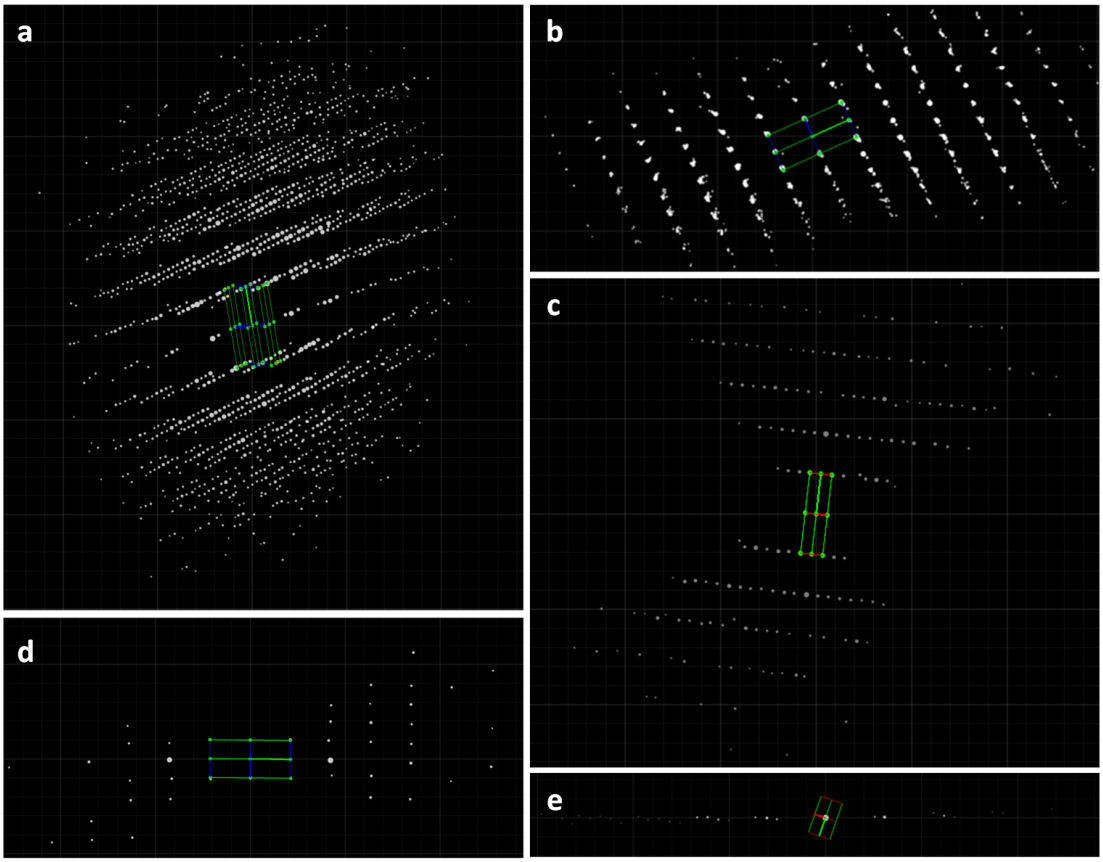

Supplementary Figure 2. Reconstructed 3D reciprocal lattice of the low-T phase from the RED data. a, The overview of 3D reciprocal lattice. **b**, The 3D reciprocal lattice along the a-axis. **c**, **d**, and **e** show the hk0, h0l, and 0kl planes. An orthorhombic unit cell could be used to index the RED data.

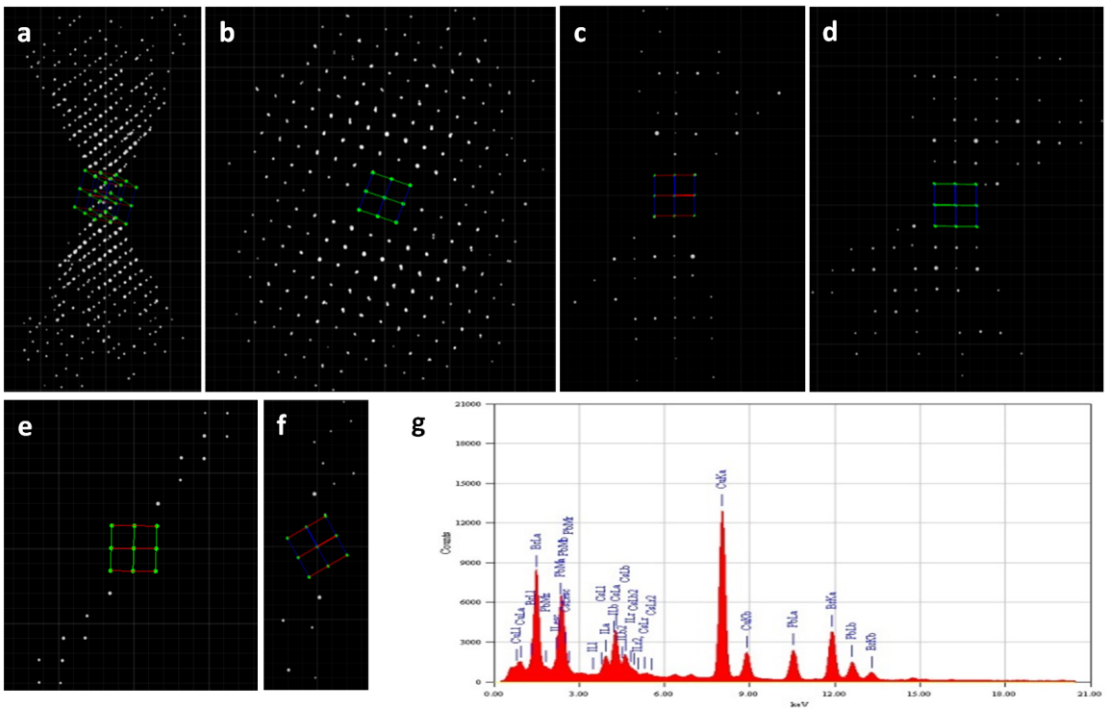

Supplementary Figure 3. Reconstructed 3D reciprocal lattice of the high-T phase from the RED data. a, The overview of 3D reciprocal lattice. **b**, The 3D reciprocal lattice along the a-axis. **c**, **d**, **e** and **f** show the hk0, h0l, 0kl, and hhl planes. A cubic unit cell has been found for the high-T phase. **g**, The EDS shows that the composition of the material is $CsPbIBr_2$ (Cu is from copper grid for TEM).

Supplementary Table 1. The refined unit cell determined by RED combined with XRD data.

Phase	**Composition**	**Space Group**	**Lattice Parameters (Å)**	**ICSD Number**
	$CsPbBr_3$	*Pmnb*	*a* = 4.597, *b* = 9.721, *c* = 16.812	28312
Low-T	$CsPbIBr_2$	*Pmnb*	*a* = 4.797, *b* = 9.982, *c* = 17.184	
	$CsPbI_3$	*Pnma*	*a* = 4.797, *b* = 10.462, *c* = 17.788	27979
	$CsPbBr_3$	*Pm*-3*m*	*a* = 5.870	97852
High-T	$CsPbIBr_2$	*Pm*-3*m*	*a* = 5.926	
	$CsPbI_3$	*Pm*-3*m*	*a* = 6.289	1627096

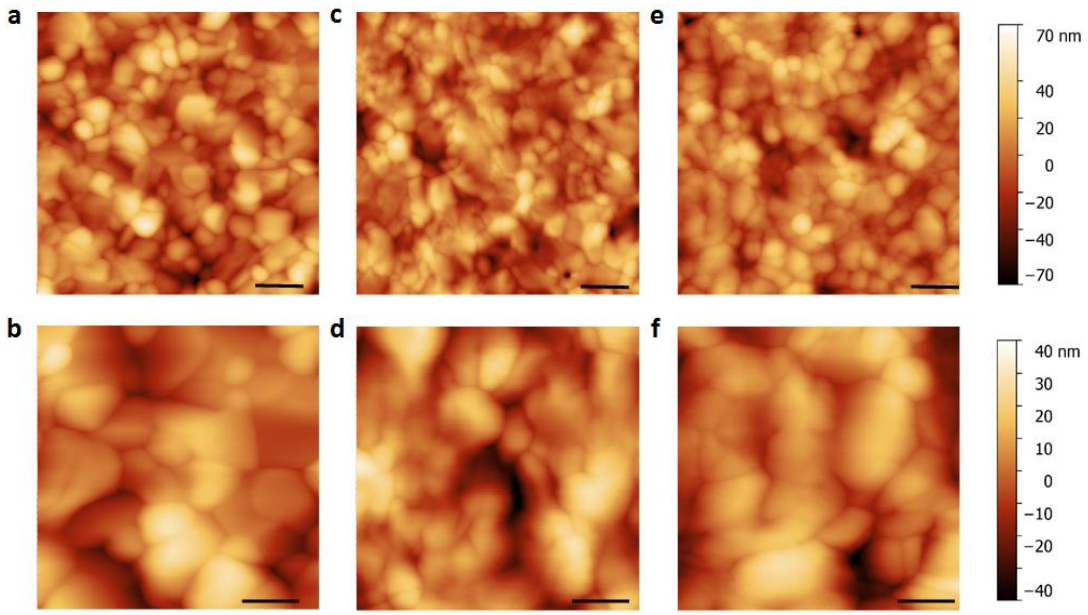

Supplementary Figure 4. AFM surface topography of the $CsPbIBr_2$ film on a NiO_x layer (without top coating). a and **b**, As-synthesized high-T phase. **c** and **d**, Moisture-induced low-T phase. **e** and **f**, Re-converted high-T phase. The freshly formed high-T phase thin film features sharp-edged grains at the surface with distinct crystallographic orientations. After moisture or heating treatment, the grain surfaces become more smooth with the appearance of some striations within the grains. Root-mean-square (RMS) factors: **a**, 15.56 nm, **c**, 16.93 nm, and **e**, 16.41 nm, respectively. Scale bars are (**a, c, e**) 500 nm and (**b, d, f**) 200 nm, respectively.

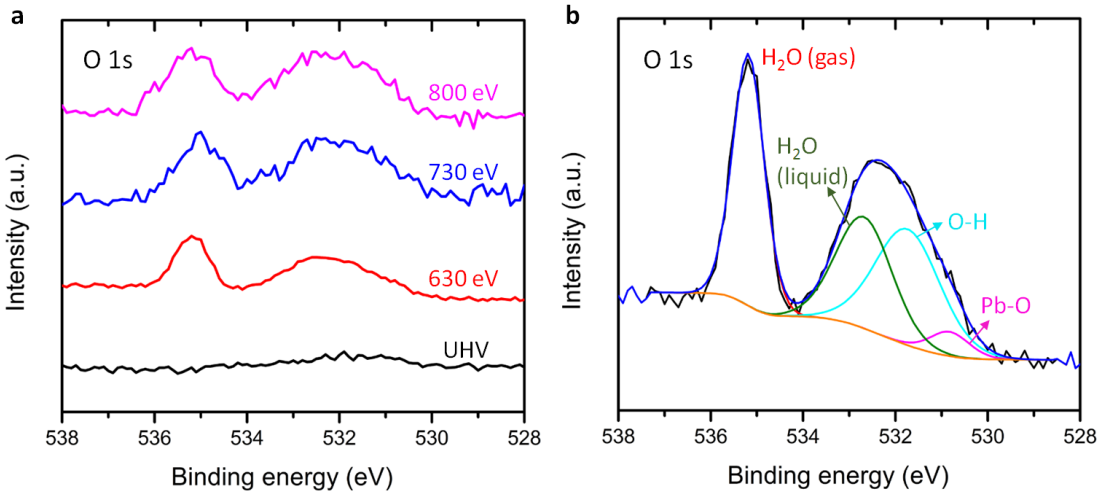

Supplementary Figure 5. In situ ambient pressure X-ray photoemission spectroscopy (AP-XPS) study. a, AP-XPS O 1s spectra of the high-T phase $CsPbI_3$ before (under UHV condition) and after exposure to H_2O (200 mTorr) and Ar (50 mTorr). At UHV condition, the O 1s peak is very weak, indicating the minimal oxygen contamination during the transfer of the sample to XPS chamber. Incident X-ray energies of 630, 730, and 800 eV were used to probe the O amount on the surface with different depth. The peak at 535.2 eV indicates the gaseous H_2O in the chamber, and its intensity would not change with time due to the consistent H_2O partial pressure in the chamber. The ratios of the surface adsorbed oxygen to gaseous H_2O at different probing depth after exposure to H_2O/Ar atmosphere are 1.825 (630 eV), 1.836 (730 eV), and 1.834 (800 eV), respectively. With increased incident X-ray energy, the surface oxygen amount has no obvious increase, indicating that H_2O is only adsorbed at the surface without diffusing into the lattice during the phase transition. **b**, Fitted AP-XPS spectrum of O 1s at 630 eV. The fitted peaks of the surface adsorbed oxygen are assigned mainly to liquid H_2O and O-H, and the lower peak to Pb-O bonding.

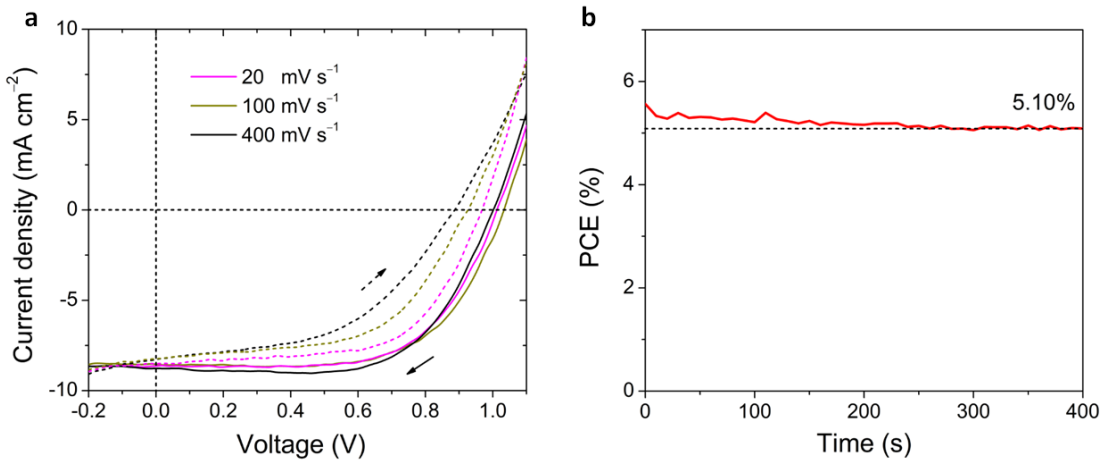

Supplementary Figure 6. Photovoltaic properties of the $CsPbIBr_2$ solar cell. a, The hysteresis behaviors under forward scan (dashed lines) and reverse scan (solid lines) directions with 20, 100, and 400 mV s^{-1} scan rates. The solar cell shows ΔPCE < 10% at a slow scan rate (20 mV s^{-1}) with respect to the scan direction. **b**, Stabilized power output under the constant voltage of 0.72 V.

Supplementary Table 2. Detailed device performance parameters corresponding to Supplementary Fig. 6a.

Scan direction	Scan rate (mV s^{-1})	J_{SC} (mA cm^{-2})	V_{OC} (V)	FF (%)	PCE (%)
Reverse scan	20	8.65	1.01	63.6	5.57
	100	8.54	1.03	64.4	5.69
	400	8.77	1.00	65.0	5.71
Forward scan	20	8.53	0.97	61.4	5.08
	100	8.24	0.93	56.3	4.30
	400	8.28	0.89	49.2	3.61

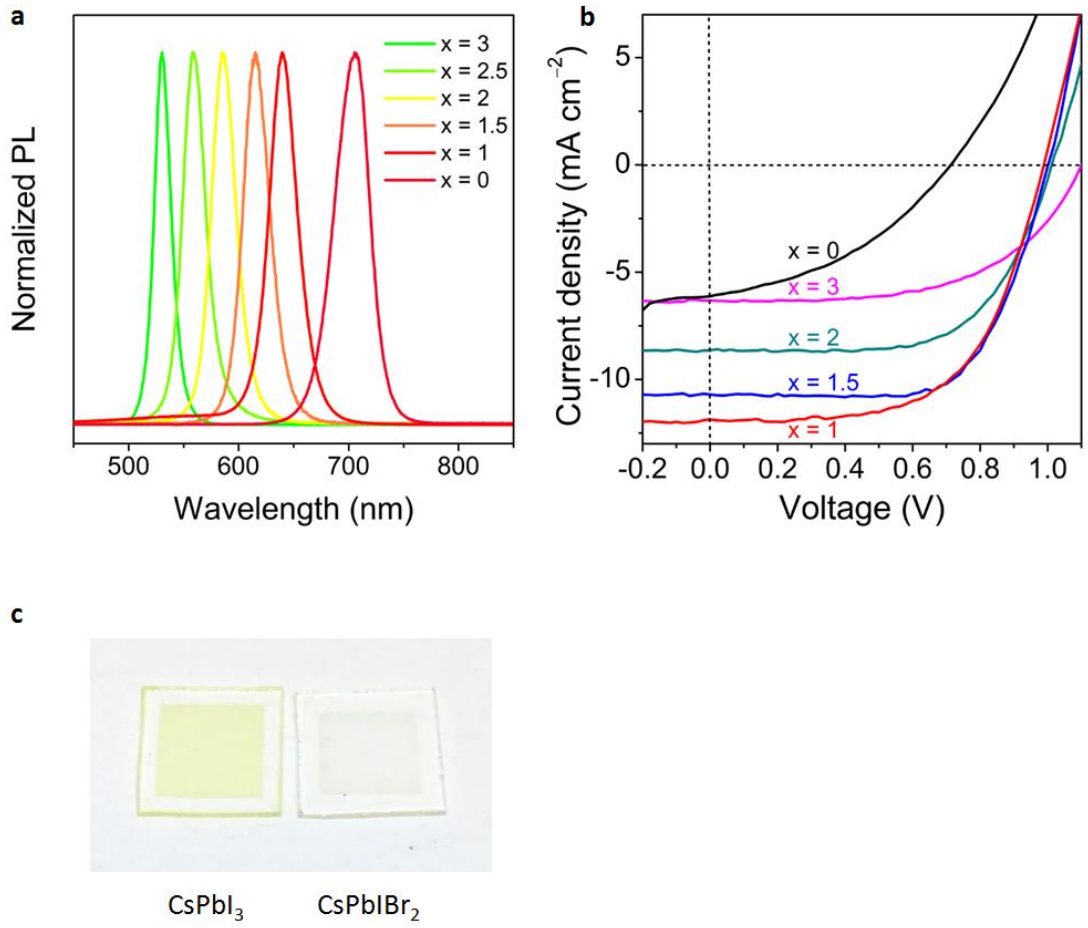

Supplementary Figure 7. The tunability of optical and photovoltaic properties of $CsPbI_{3-x}Br_x$ films. a, PL spectra with different compositions (x = 0, 1, 1.5, 2, 2.5, and 3), showing spectral tunability across 530−705 nm. It is noted that high intensity laser beams may induce phase segregation during PL measurement. **b**, J-V curves of solar cell devices with different halide compositions (reverse scan at 20 mV s^{-1}). **c**, The photographs of the low-T phase $CsPbI_3$ (left) and $CsPbIBr_2$ (right) thin films. The $CsPbI_3$ low-T phase exhibits the yellow color, which is why it's colloquially called the "yellow phase", while the $CsPbIBr_2$ film we demonstrated here appears colorless in the low-T state.

Supplementary Table 3. Detailed device performance parameters corresponding to Supplementary Fig. 7b.

Scan direction	Composition *x*	J_{SC} (mA cm^{-2})	V_{OC} (V)	FF (%)	PCE (%)
Reverse scan	0	6.12	0.71	39.1	1.71
	1	11.86	0.99	60.5	7.10
	1.5	10.61	1.00	68.0	7.23
	2	8.65	1.01	63.6	5.57
	3	6.32	1.10	57.5	4.00
Forward scan	0	5.91	0.70	37.3	1.54
	1	11.42	0.98	57.9	6.47
	1.5	10.50	0.96	64.2	6.50
	2	8.53	0.97	61.4	5.08
	3	6.17	1.08	56.7	3.77

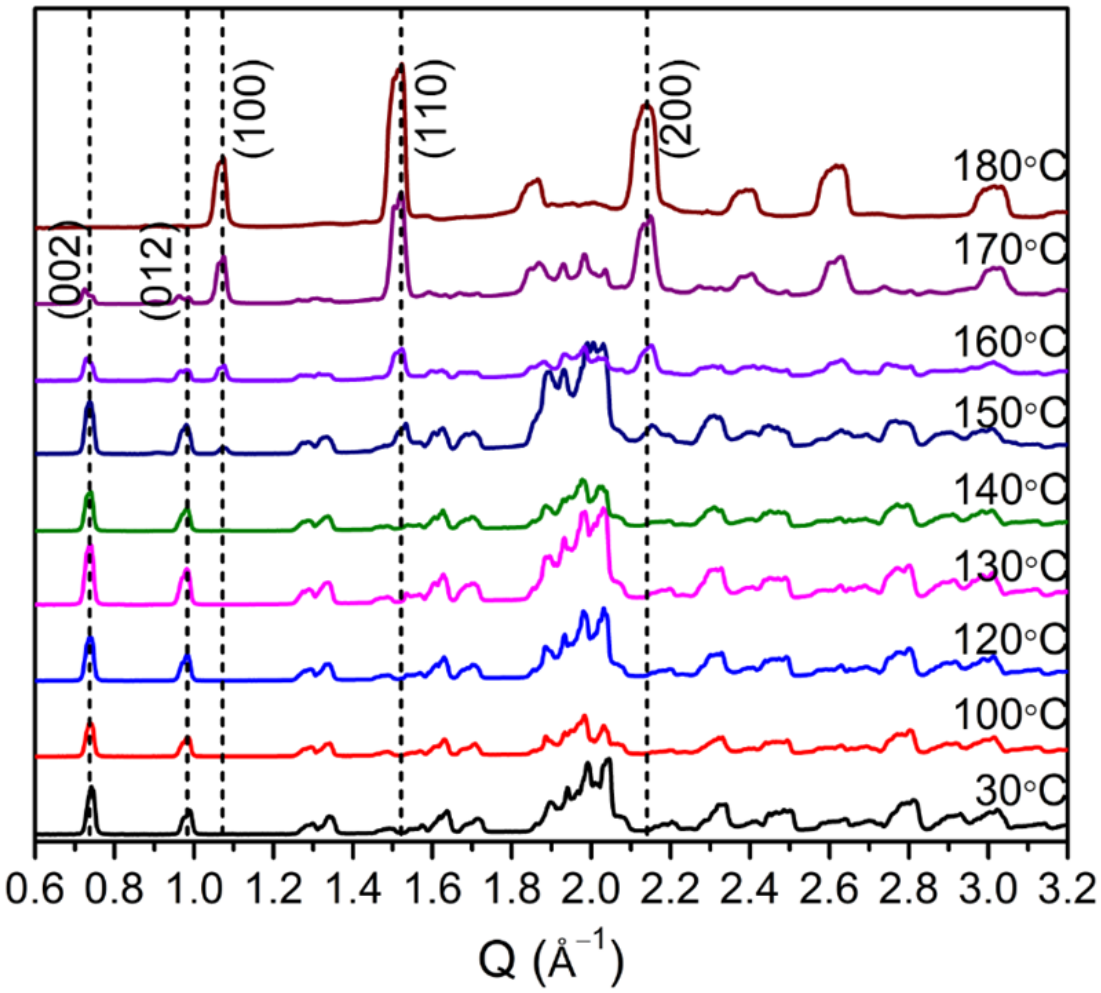

Supplementary Figure 8. Variable-temperature GIWAX measurement. The $CsPbIBr_2$ thin film shows a low-T to high-T phase transition starting at ~150 ℃.

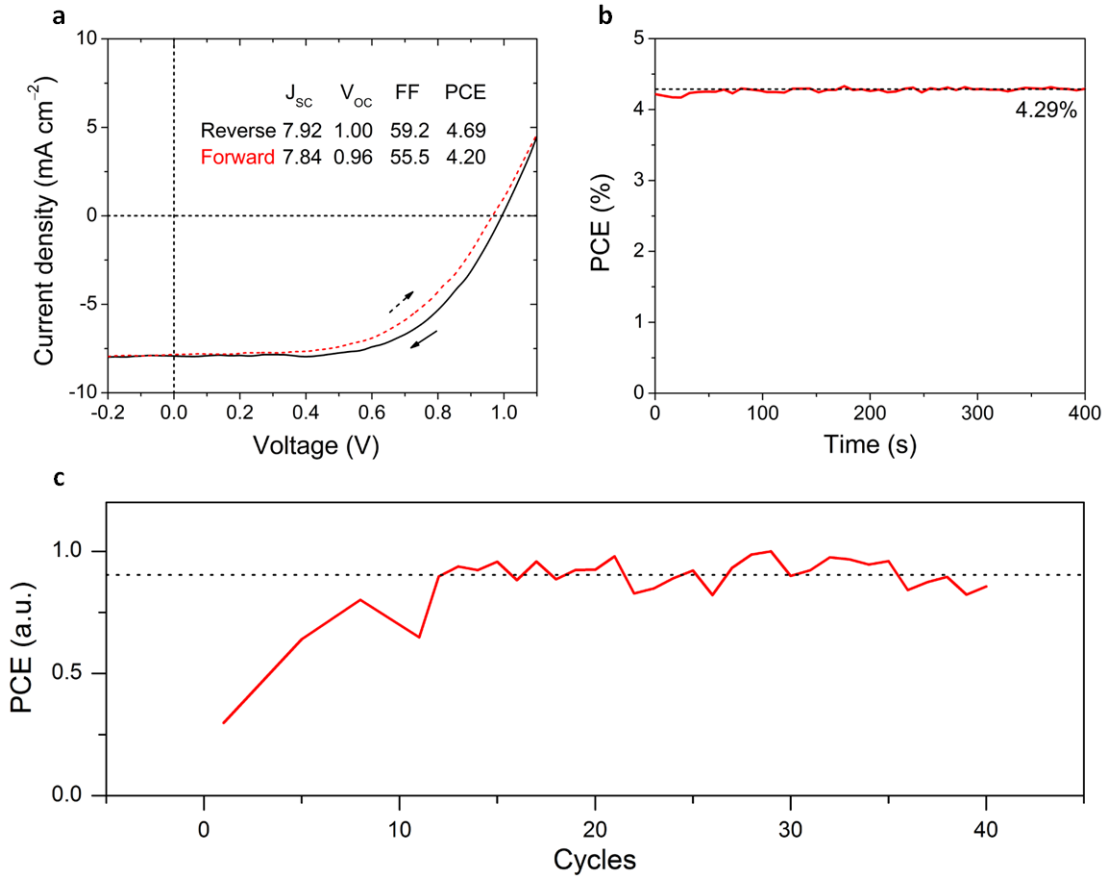

Supplementary Figure 9. Photovoltaic properties of the semi-transparent solar cell. a, The hysteresis behavior under forward scan (dashed line) and reverse scan (solid line) directions (20 mV s^{-1}). **b**, Stabilized power output under the constant voltage of 0.70 V. **c**, The power conversion efficiency (PCE) of the high-T phase over 40 transition cycles. In the initial several cycles, we observed an improvement in performance of the semi-transparent device, which is probably due to the improved crystallinity of the interlayer materials and the top ITO electrode.

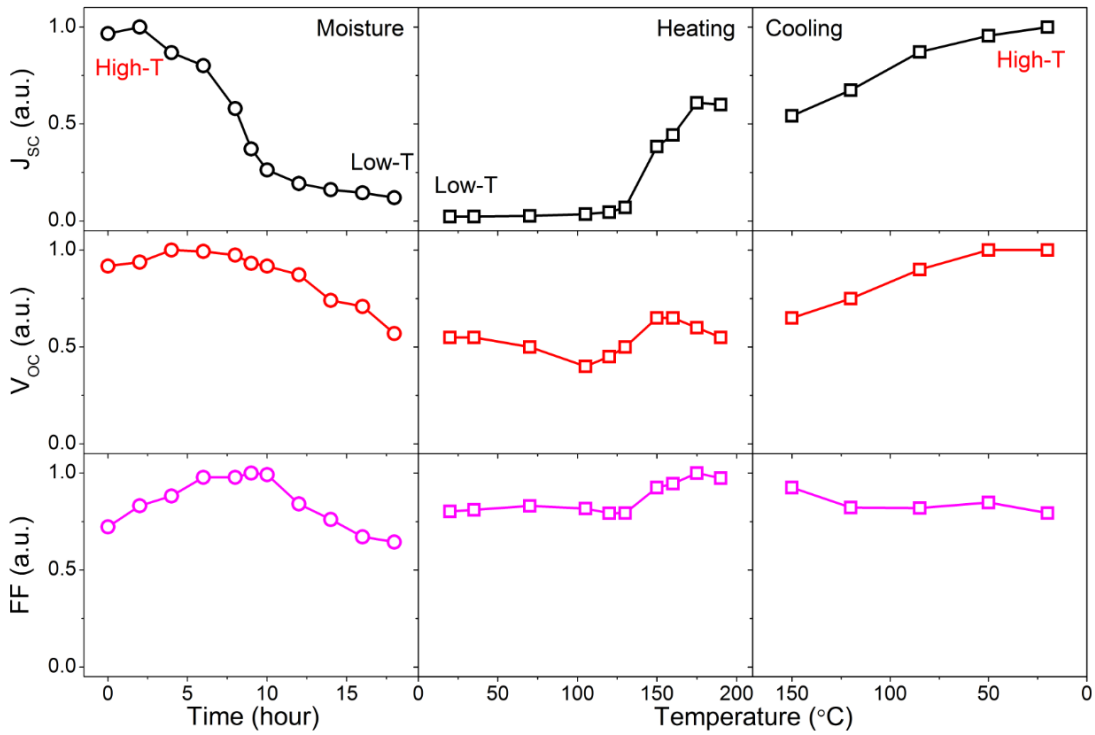

Supplementary Figure 10. In situ observation of the evolution of the device performance. Variations of short-circuit current density (J_{SC}), open-circuit voltage (V_{OC}), and fill factor (FF) of the $CsPbIBr_2$ solar cell during the high-T to low-T and low-T to high-T phase transitions.

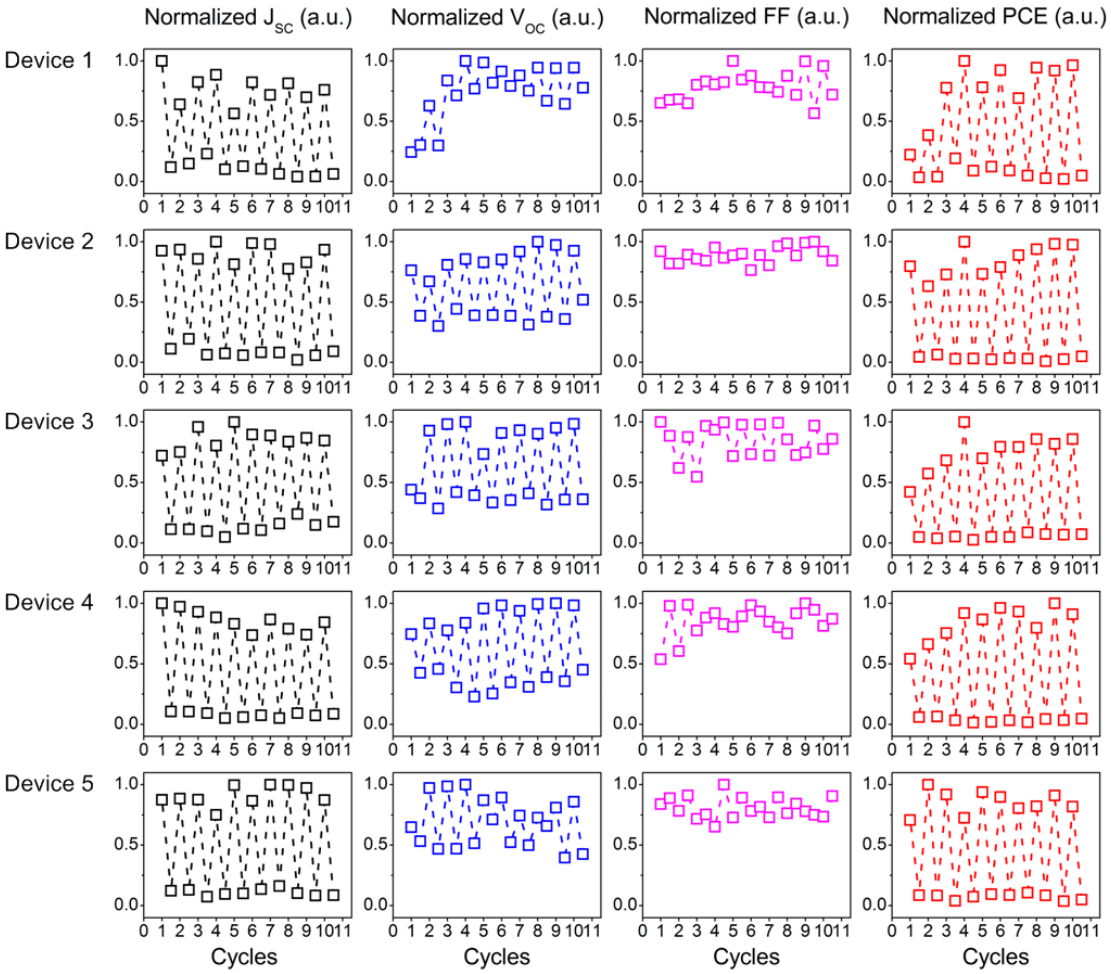

Supplementary Figure 11. The performance reversibility of the $CsPbIBr_2$ solar cells. The photovoltaic properties of five representative devices show similar variation trends during cycling.